Couette-Poiseuille flow based non-linear flow over a square cylinder near plane wall

Rajesh Bhatt[1a], Dilip K. Maiti[2b], Md. Mahbub Alam[*1] and S. Rehman[3c]

[1]*Institute for Turbulence-Noise-Vibration Interaction and Control, Shenzhen Graduate School, Harbin Institute of Technology, Shenzhen, China*
[2]*Department of Applied Mathematics with Oceanology and Computer Programming, Vidyasagar University, Midnapur 721102, India*
[3]*Center for Engineering Research, Research Institute, King Fahd University of Petroleum and Minerals, Dhahran-31261, Saudi Arabia*

Abstract. A numerical study on the flow over a square cylinder in the vicinity of a wall is conducted for different Couette-Poiseuille-based non-uniform flow with the non-dimensional pressure gradient P varying from 0 to 5. The non-dimensional gap ratio L ($=H^*/a^*$) is changed from 0.1 to 2, where H^* is gap height between the cylinder and wall, and a^* is the cylinder width. The governing equations are solved numerically through finite volume method based on SIMPLE algorithm on a staggered grid system. Both P and L have a substantial influence on the flow structure, time-mean drag coefficient $\overline{C}_D$, fluctuating (rms) lift coefficient (C_L'), and Strouhal number St. The changes in P and L leads to four distinct flow regimes (I, II, III and IV). Following the flow structure change, the $\overline{C}_D$, C_L', and St all vary greatly with the change in L and/or P. The $\overline{C}_D$ and C_L' both grow with increasing P and/or L. The St increases with P for a given L, being less sensitive to L for a smaller P (< 2) and more sensitive to L for a larger P (> 2). A strong relationship is observed between the flow regimes and the values of $\overline{C}_D$, C_L' and St. An increase in P affects the pressure distribution more on the top surface than on bottom surface while an increase in L does the opposite.

Keywords: square cylinder; couette-poiseuille flow; aerodynamic characteristics; gap flow

1. Introduction

In many practical cases the flow approaching the structures, for example offshore platforms, is not uniform because of the wall (seabed) shear stress. Although high Reynolds number flows appear in most practical examples (e.g., Alam *et al.* 2011, Alam and Zhou 2013, Rastan *et al.* 2017), the flow at a low Reynolds number has an application in small heat exchangers and electronic cooling components. While the mean flow over a square cylinder subjected to a uniform flow is symmetric about the wake centerline, that subjected to a non-uniform is asymmetric. The difference in the flow velocities over the upper and lower surfaces of the cylinder is responsible for the asymmetry. The wall proximity effect makes the flow more complex than without the wall, resulting in different wake flow patterns. It is, therefore, crucial to understand the basic

flow phenomena for a cylinder under the influence of non-uniform flow near the wall. This study investigates the flow characteristics of a square cylinder when the gap height L ($= H^*/a^*$, where H is the gap between the wall and the cylinder and a^* is the height of the cylinder) and non-linearity of the approaching velocity profile (based on inlet pressure gradient P) are varied.

Numerical studies on the flow past a square cylinder for different inlet shear parameter K and at different Reynolds numbers Re were conducted by Hwang and Sue (1997, $Re = 500 - 1500$, $K = 0 - 0.25$), Cheng *et al.* (2005, $Re = 100$, $K = 0 - 0.5$), Cheng *et al.* (2007, $Re = 50 - 200$, $K = 0 - 0.5$), and Lankadasu and Vengadesan (2008, $Re < 100$, $K = 0 - 0.2$). Their results showed that the Strouhal number (St), time-mean drag coefficient ($\overline{C}_D$) and fluctuating forces all decrease with increasing K. Lankadasu and Vengadesan (2008) reported that, with increasing K, the critical Re, at which flow becomes unsteady, is reduced. Similarly, several numerical studies have been carried out on a rectangular cylinder of different aspect ratios under a uniform shear flow ($P = 0$), e.g., by Sohankar (2008, $Re = 10^5$), Islam *et al.* (2012, $Re = 100-250$), Yu *et al.* (2013, $Re = 10^5$) and Cao *et al.* (2014, $Re = 22000$). These studies have shown that the Re effect is less significant compared to other parameters (e.g., incoming velocity profile). Cao *et al.* (2014) concluded that, with increasing K, the stagnation point linearly shifts to the high-velocity side, which was

---

*Corresponding author, Professor
  E-mail: alamm28@yahoo.com
[a] Post-Doctoral
  E-mail: rajesh_tolibans@yahoo.com
[b] Professor
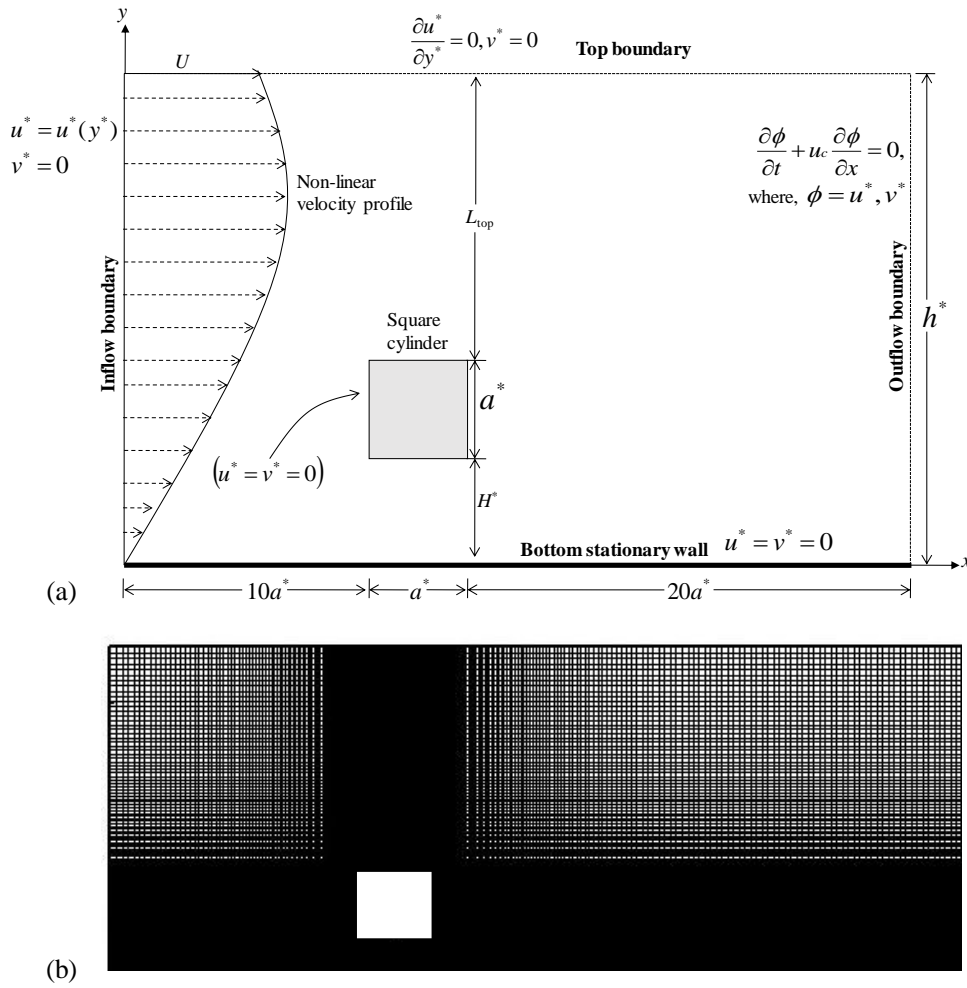 E-mail: d_iitkgp@yahoo.com
[c] Professor
  E-mail: srehman@kfupm.edu.sa

$$\frac{\partial u^*}{\partial y^*}=0, v^*=0 \quad \text{Top boundary}$$

$u^* = u^*(y^*)$
$v^* = 0$

Non-linear velocity profile

L_{top}

$$\frac{\partial \phi}{\partial t}+u_c\frac{\partial \phi}{\partial x}=0,$$
$$\text{where, } \phi = u^*, v^*$$

h^*

Square cylinder

a^*

$(u^* = v^* = 0)$

H^*

Bottom stationary wall $\quad u^* = v^* = 0$

(a) $\longleftarrow 10a^* \longrightarrow \longleftarrow a^* \longrightarrow \longleftarrow 20a^* \longrightarrow$

(b)

Fig. 1 (a) Schematics of the computation domain and boundary conditions and (b) Typical grid system around the cylinder for $L = 0.5$

identified to be an inherent behavior of the flow around a cylinder subjected to a shear flow.

Several studies on the wall proximity effect on a cylinder flow have also been carried out (Bailey *et al.* 2002, Lee *et al.* 2005, Kumaran and Vengadesan 2007, Wang and Tan 2008, Dhinakaran 2011, Maiti 2012, Samani and Bergstorm 2015). Bailey *et al.* (2002) conducted an experimental study and examined the vortex shedding from a square cylinder near a wall at $Re = 1.9 \times 10^4$. Their results showed that the suppression of vortex shedding occurs for $L < 0.4$. Lee *et al.* (2005) studied the effect of cylinder aspect ratio and L ($0.3 \leq L \leq 2$), introducing a simple passive control method to reduce the aerodynamic drag and vortex-induced vibration. They observed that the vortex begins to shed by the interaction of the upper shear layer with the upwash flow from the gap. Wang and Tan (2008) experimentally compared the near-wake flow patterns for a circular and a square cylinder for $L = 0.1 - 1.0$. They concluded that the vortex shedding strength for the square cylinder is relatively weaker, as compared to that for the circular cylinder at the same L. The critical L for the onset of vortex shedding is found to be 0.3 and 0.5 for the circular

and square cylinders, respectively. Maiti (2012) reported that aerodynamic characteristics of a square cylinder under a uniform shear flow are more sensitive to L for $L > 1$ than for $L \leq 1.0$. Dhinakaran (2011) observed an increase in aerodynamic forces with decreasing L for a square cylinder placed near a moving wall at $Re = 100$. The flow behavior was classified into two-row vortex street ($1 \leq L \leq 4$), single-row vortex street ($0.4 \leq L \leq 1$), quasi-steady vortex street ($L = 0.3$) and vortex shedding suppression ($L < 0.3$). Recently, Samani and Bergstrom (2015) conducted large eddy simulation to examine the wall proximity effect of a square cylinder for three values of $L = 0, 0.5$ and 1.0 at $Re = 500$. An increase in L leads to an increase in time-mean lift coefficient ($\overline{C}_L$) and a decrease in $\overline{C}_D$. As the cylinder approaches the wall, the wake flow becomes increasingly asymmetric with the top recirculation cell displaced significantly upward and further downstream, and a secondary recirculation zone develops on the bottom wall.

The aforementioned studies on the flow around a single cylinder are based on either a uniform flow or a linear shear flow with and without wall proximity. It is clear from these studies that the inlet velocity profile and the gap flow
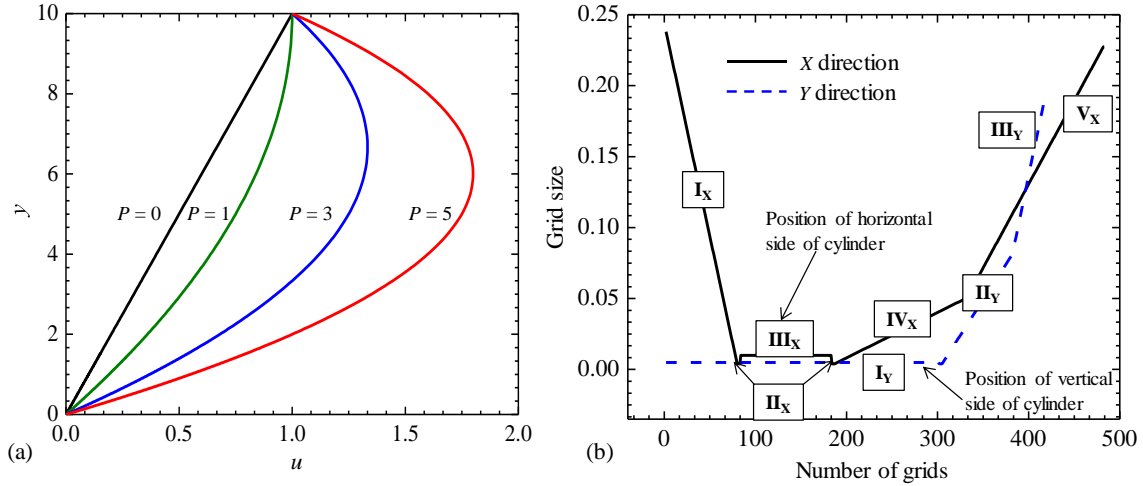
Fig. 2 (a) Couette-Poiseuille flow based nonlinear incident velocity profiles for different *P* and (b) Typical grid distribution for *L* = 0.5

greatly alter the aerodynamic forces and hence the flow around the cylinder. However, numerical studies on a square cylinder in a wall proximity under a non-uniform shear flow are scarce. Therefore, the present study aims to understand the effect of inlet non-linear velocity profile on aerodynamic forces and the wake flow structure of a square cylinder at different *L*.

2. Problem formulation

With the wall lying along the x*-axis, a cylinder of a square cross-section of a height *a** is placed parallel to the wall at gap height *H** from the wall (Fig. 1). Following the previous studies (e.g., Bhattacharyya and Maiti 2005), the inlet and outlet boundaries were placed at a distance of 10*a** and 20*a** from the front and rear faces of the cylinder, respectively. The top lateral boundary lies at 10*a** from the plane wall. The inlet flow field is taken as Couette-Poiseuille flow based nonlinear velocity profile *u**(y*)*. This upstream condition is consistent with the Navier-Stokes equation and viscous effects because of the no-slip requirement at the wall (Schlichting and Gersten 2000). In other words, the cylinder is submerged into the boundary layer of the plane wall. The following nonlinear velocity profile (with characteristic velocity *U* at *y** = 10*a**) described by Schlichting and Gersten (2000) is considered at the inlet

$$\frac{u^*}{U} = \frac{y^*}{h^*} + P\frac{y^*}{h^*}\left(1 - \frac{y^*}{h^*}\right) \tag{1}$$

where *U* is the velocity at a distance *h** from the wall, and *P* is the nondimensional pressure gradient. The *P* is defined as

$$P = \frac{h^{*2}}{2\mu U}\left(-\frac{dp^*}{dx^*}\right) = \frac{1}{2}h^2 Re\left(-\frac{dp}{dx}\right) \tag{2}$$

where *Re* = *Ua**/ν, *p* = *p**/(ρU²) and, *μ* and *ν* are the

viscosity and kinematic viscosity of the fluid. Different nondimensional velocity profiles *u(y)* for different values of *P* with fixed height *h** = 10*a** are presented in Fig. 2(a).

2.1 Governing equations and numerical method

The non-dimensional Navier-Stokes equations for a two-dimensional laminar flow are given by

$$\nabla \cdot V = 0 \tag{3}$$

The nondimensional quantities *V* = (*u*, *v*), *p* and *t* denote the velocity, pressure and time, respectively, where *a** and *U* are used as the characteristic length and velocity scales for the normalization.

$$\frac{\partial V}{\partial t} + (V \cdot \nabla)V = -\nabla p + \frac{1}{Re}\nabla^2 V \tag{4}$$

The no-slip condition is used on the cylinder surfaces and on the plane wall. A Dirichlet boundary (*u* = *u(y)*, *v* = 0) is used at the inlet boundary, while the Sommerfeld condition ((∂ϕ/∂t)+*u_c*(∂ϕ/∂x) = 0, where *ϕ* is any flow variable, and *u_c* is the local wave speed) is applied at the outlet. A slip boundary condition (∂u/∂y = 0, *v* = 0) is imposed on the top lateral boundary. The numerical treatment to the Sommerfeld condition has been discussed in details in Maiti (2011).

A finite volume method on a staggered grid system and then the pressure correction based iterative algorithm SIMPLE (Patankar 1980) are applied. A third-order accurate QUICK (Leonard 1995) is employed to discretize the convective terms and central differencing scheme for diffusion terms. A fully implicit second-order scheme is incorporated to discretize the time derivatives. At the initial stage of motion, times step is taken to be 0.0001 which has been subsequently increased to 0.001 after the transient state.
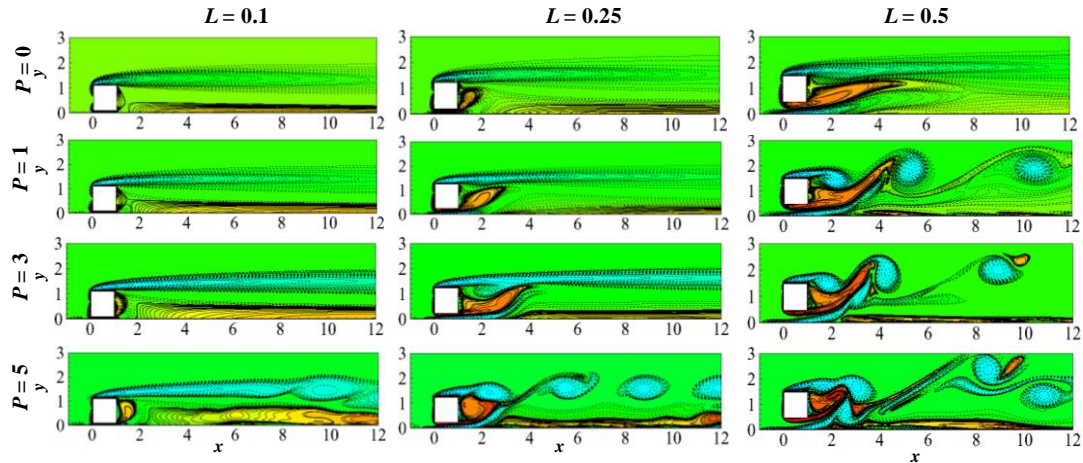
Fig. 3 Instantaneous vorticity contours at different gap heights ($L \leq 0.5$) for different P. The solid and dashed lines represent the positive and negative vorticities, respectively

3. Grid independence and validation of code

A nonuniform grid distribution is considered in the domain, with a uniform grid on the cylinder surface and increasingly enlarged grids away from the cylinder surface. The grid distribution in x and y directions is shown in Fig. 2(b), similar to that used in the previous study (Bhattacharyya and Maiti 2004, Maiti 2011, 2012). Depending on the size of the distributed grids, the horizontal and vertical lines of the computational domain are divided into five and three, respectively, distinct segments. Along the y-direction, a uniform grid with size $0.005a*$ is considered between the wall and top of the cylinder (within the segment 'I_y' in Fig. 2(b)). With reference to Franke *et al.* (1990) and Sohankar *et al.* (1997), the value of the first grid size from the cylinder surface is kept constant as $0.004a*$ for the present computation.

The grid refinement study on the number of uniform nodes and on the resolution of grid near the cylinder surface and the far fields was conducted in the previous study (Maiti, 2011, 2012, Maiti and Bhatt, 2015) for the case of single and two tandem cylinders. A detailed discussion on the percentage of deviation has been made in these studies. In the present study, the grid distribution along the y-direction is varied according to the gap height of the cylinder from the wall. The numerical code validated for the case of a square cylinder placed near a wall (Bhattacharyya *et al.* 2006) is used in the present study. Thus, the previously published results by the authors also show the validity of the used code for this work.

In the present study the following operational dimensionless parameters affecting the flow are considered:

- L = 0.1, 0.25, 0.5, 1.0, 1.5 and 2.0
- Inlet pressure gradient P = 0, 1, 3 and 5
- Reynolds number Re = 1000, based on the velocity at height $10a*$ from the wall (Maiti and Bhatt 2015). Davis and Moore (1982), Davis *et al.* (1984) presented 2D numerical results for square and rectangular cylinders and found a good agreement between the numerical and experimental results for Re up to 1000 for a

uniform flow. They concluded that the use of more grid points could extend the range of Re for 2D computation. Bailey *et al.* (2002) concluded that the vortex formation process is increasingly two dimensional for a square cylinder in the vicinity of a plane wall. The same opinion was shared by Zovatto and Pretizetti (2001), Bhattacharyya and Maiti (2005), Maiti (2011, 2012). Bhattacharyya and Maiti (2004), Maiti (2011) presented the 2D numerical results of a square cylinder for L = 0.5 at Re up to 1000.

4. Results and discussion

The effect of L and P on the flow and aerodynamic characteristics of a square cylinder is discussed here. The results of vorticity contours, power spectra, and pressure distributions are presented and discussed.

4.1 Flow structure

Fig.3 shows the instantaneous vorticity contours for $L \leq 0.5$. At L = 0.1, $P \leq 3$, the flow is steady. As P is increased from 3 to 5, unsteadiness is developed in the far field and propagates towards the cylinder, and the flow becomes quasi-steady in nature. The flow through the gap is very small. On the other hand, the gap flow is significant at L = 0.25. The flow is steady at $P \leq 1$ (L = 0.25), the upper shear layer being straight and the gap flow generating an anticlockwise recirculation behind the cylinder. At P = 3, the gap flow recirculation region is stretched upward and results in a clockwise recirculation of a part of the upper shear layer. The flow still remains steady. A more detailed explanation of vortex shedding suppression from a square cylinder at a lower L can be found in Martinuzzi *et al.* (2003) and Maiti (2012). For P = 5, the upper shear layer gets sufficient momentum to shed vortices while the gap flow with an anticlockwise recirculation has a quasi-steady nature. Hence, the wake is dominated by a single row of clockwise vortices with a definite peak in the spectra of lift coefficient, which will be shown later.
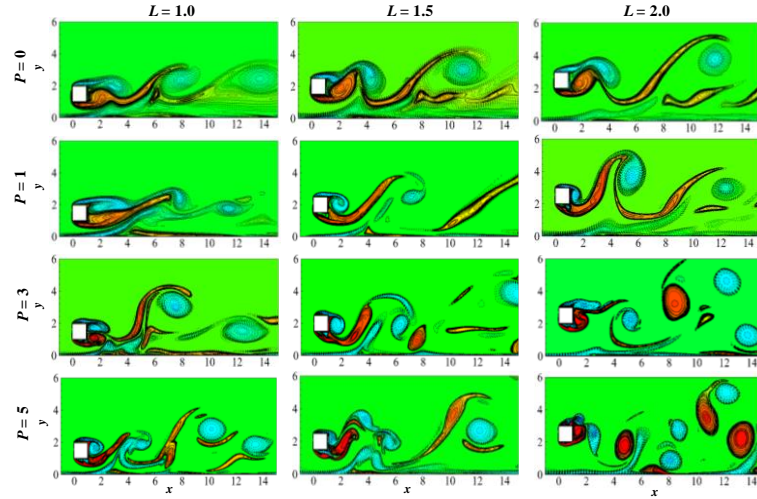
Fig. 4 Instantaneous vorticity contours at different gap heights ($L \geq 1.0$) for different P. The solid and dashed lines represent the positive and negative vorticities, respectively

Upon increasing L to 0.5, the flow is yet steady for $P = 0$ and the gap flow recirculation region gets bigger than that at a smaller L. Wang and Tan (2008)'s experimental study done for $P = 0$ revealed that the critical L for the onset of vortex shedding is 0.5. At $P = 1$, the shear layers of different vorticity strengths from the upper and lower sides of the cylinder curl up into vortices in an alternating fashion. While the vortices from the lower side and from the wall elongate and dissipate faster in the wake, those from the upper side are regular in size and appearance. A single row of vortices emanating from the upper side of the cylinder thus characterizes the wake. This flow type can be regarded as regular vortex shedding from the upper side, i.e., $W_{U,R+L,0}$, where subscript 'U', 'R', 'L', and '0' stand for 'upper', 'regular', 'lower' and 'no-vortex', respectively, while 'W' denotes 'wake'. That is, $W_{U,R+L,0}$ means that regular vortex from the upper side preserves in the wake but no vortex from the lower side survives or sheds. A strong interaction between the upper vortex and two counter-rotating gap vortices leads to the dissipation of the gap vortices. Zovatto and Pedrizzetti (2001) reported that an interaction of the wall boundary layer with the lower shear layer suppresses the positive vortices from the lower side of the cylinder, the downstream wake featuring a row of negative vortices. Compared to the counterpart of the unsteady flow for $L = 0.25$, $P = 5$, the streamwise distance between the consecutive vortices is larger for $L = 0.5$, $P = 1$. With increasing P from 1 to 5 ($L = 0.5$), the formation of vortices occurs closer to the cylinder, and the gap vortices are less stretched during their formation. Now following the definitions of the single row street wake ($W_{U,R+L,0}$), the steady flow can be expressed as $W_{U,0+L,0}$, i.e., no vortices in the wake from the upper and lower sides.

Li *et al.* (2017) for $P = 0$ numerically studied the wall effect ($0 \leq L \leq 2.0$) on an inclined flat plate at an angle of 20° with the ground plane. They reported that when L is decreased from 2 to 0.5 the positive vortex clusters generated from the trailing edge flattens and the vortex strength weakens. As a result, only negative vortices were observed in the downstream flow. A Further decrease in L yields a steady flow.

Fig. 4 shows instantaneous vorticity structures at $L = 1.0$, 1.5 and 2.0 for different values of P. The vortex shedding commences for $L = 1.0$, $P = 0$. The interaction occurs between the vortices where the upwash flow from the gap facilitates the interaction, and a row of negative vortices features the wake, i.e., $W_{U,R+L,0}$. An increase in L results in an increase in the local Reynolds number that is mechanically similar to an increase in P since $(-dP/dx) = 2P$ $(1/h)^2(1/Re)$, where h is the nondimensional height from the wall. With an increase in P the interaction of positive and negative vortices leads to an irregular arrangement of vortices in the wake, making wake vortices different in size and intensity. A dramatic change takes place when L is increased further to 1.5 for $P = 1$. The roll-up is delayed of the shear layer from the lower surface of the cylinder, the positive vortices from the gap becoming more stretched and surviving in the wake (see snapshot for $L = 1.5$, $P = 1$). Here this flow is termed as $W_{U,R+L,S}$; here subscript 'S' stands for 'stretched'. In other words, $W_{U,R+L,S}$ means the wake is characterized by regular vortices from the upper side and stretched vortices from the lower side of the cylinder. For a higher P, the vortices from the lower side become stronger and survive in the wake as regular vortices. A further increase in L to 2.0 results in the lower side vortices to stretch more for a small P ($P = 0$, 1; $L = 2.0$) but to be regular in size and appearance at a large P ($P = 3$ and 5; $L = 2.0$). The wake for $P = 3$, 5 at $L = 2.0$ thus characterizes $W_{U,R+L,R}$, i.e., regular vortices from both upper and lower sides. At a larger L there is a pronounced flow separation of the shear layers from the wall, disseminating negative vortices. It triggers the instability in the vortex distribution in the wake, and the wake unsteadiness enhances. It is clear from Figs. 3 and 4 that the flow structure strongly depends on L and P. With the increase in L, the front stagnation point of the cylinder moves to the higher velocity side and the flow is biased towards the lower velocity side.
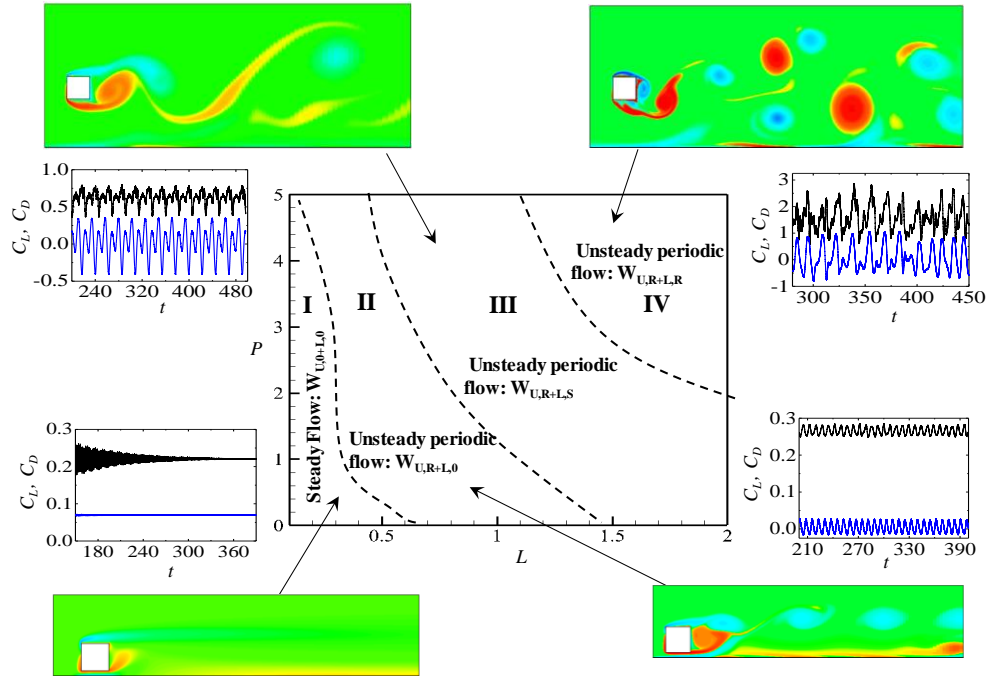
Fig. 5 Classification of flow structures in the *P-L* plane and representative vorticity contours and corresponding time histories of C_D (black line) and C_L (blue line). The dashed lines represent the boundaries between the regimes
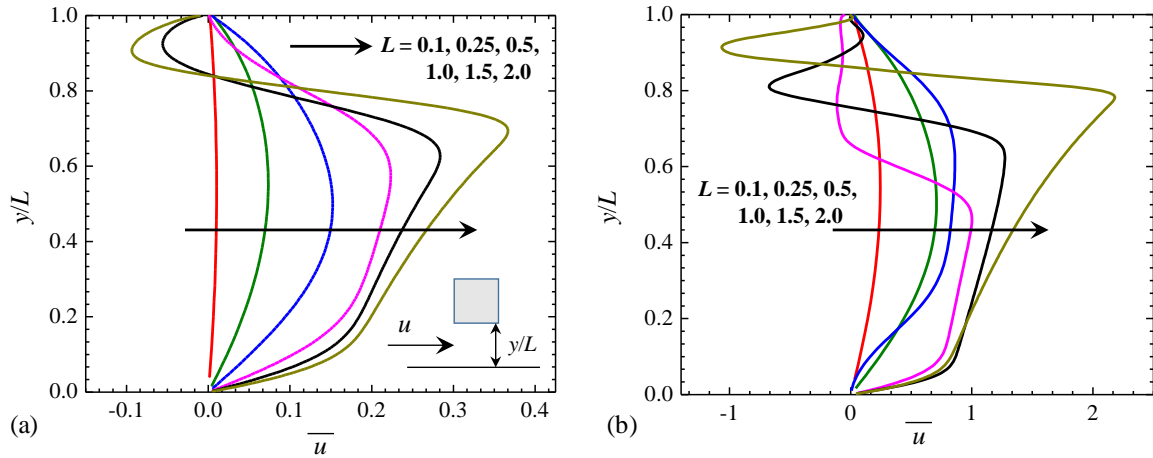

Fig. 6 Time-mean streamwise velocity profiles for various *L* at the exit of the gap between the cylinder lower surface and the wall. (a) *P* = 0 and (b) *P* = 5

Based on the above discussion, four distinct flow patterns are identified in a broad sense. They are steady flow $W_{U,0+L,0}$ (regime I) and unsteady flows $W_{U,R+L,0}$ (regime II), $W_{U,R+L,S}$ (regime III), and $W_{U,R+L,R}$ (regime IV), respectively, as marked in the *P-L* plane in Fig. 5. Representative flow structures and corresponding drag and lift (C_D and C_L) histories are shown for each flow regime. The time histories of C_D and C_L, and the wake flow all indicate the steady flow at small *L* (regime I). The steady flow regime is wide at a small *P* and narrow at a high *P*. When *L* is increased for a given *P*, the flow becomes unsteady (regime II). In this flow pattern the vortices from

the lower side rapidly dissipate. The wake is characterized by a single row of vortices ($W_{U,R+L,0}$). The variations in C_L and C_D thus regular. For a further increase in *L* (regime III), the lower side of the cylinder disseminates stretched vortices in the wake, while the upper side spawns regular vortices ($W_{U,R+L,S}$). The time evolutions of C_D and C_L are thus not symmetric about their mean. Regime IV appears at a high *P* and *L*, where regular vortices are released from both sides of the cylinder. Accordingly, the symmetry of the C_D and C_L about their mean improves.
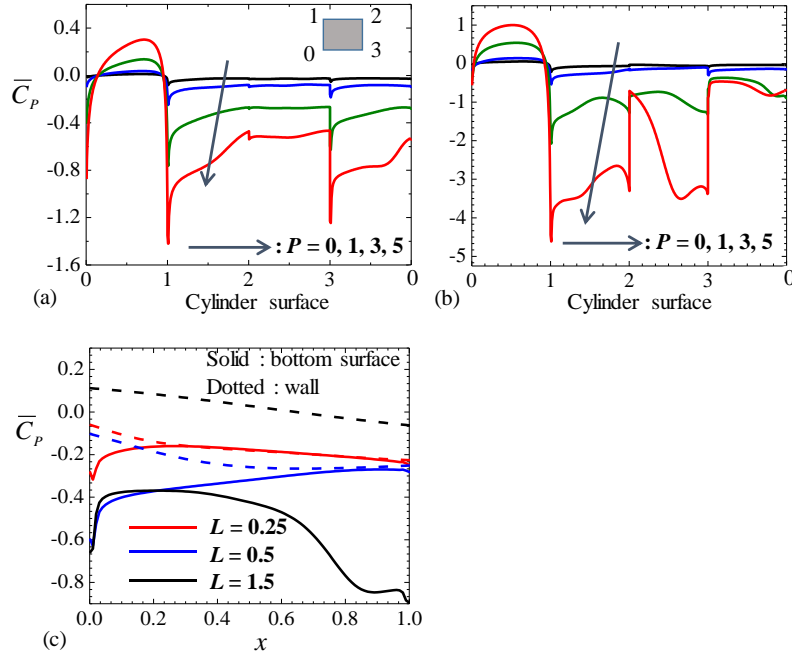
Fig. 7 Time-averaged pressure coefficient ($\overline{C}_P$) on the cylinder surface. (a) $L = 0.5$, and (b) $L = 1.5$. (c) Pressure distribution along the wall and the lower surface of the cylinder at different L for $P = 3$

4.2 Gap flow

It is clear from the discussion made above that both L and P affect the flow structure behind the cylinder. It is therefore instructive to investigate the velocity profile in the gap region for different P to understand the wake structure. Fig. 6 shows the mean velocity profiles for different L and P. Lee *et al.* (2005) reported that in the cases where the vortex shedding occurs, the velocity in the gap is greater than that without vortex shedding. Also, the position at which maximum velocity occurs is closer to the lower surface of the cylinder. Presently, for $L \leq 0.5$ at $P = 0$, the gap flow is similar to a jet flow, the velocity profile taking a parabolic shape owing to a steady flow. As observed in Fig. 4, the flow becomes unsteady for $L \geq 1.0$ at $P = 0$. The gap flow for the unsteady cases ($L \geq 1.0$, Fig. 6(a)) is biased towards the cylinder, and the position of the maximum velocity shifts closer to the cylinder. The interaction between vortices from the cylinder and wall causes the upward flow near the trailing edge of the cylinder. The flow velocity near the cylinder surface is negative for $L = 1.5$ and 2.0 because of the recirculating flow between the shear layer and lower surface. On the other hand, though the flow is unsteady for $L = 1.0$, recirculating flow is absent as the shear layer is attached to lower surface and separates from the trailing edge (Fig. 4). At $P = 5$ (Fig. 6(b)), an increase in the mean velocity in the gap region prevails and vortex shedding occurs at relatively a smaller L, compared to the $P = 0$ counterpart. A larger L corresponds to a higher flow for $y/L < 0.5$. Again the recirculating flow crops up for $L \geq 1.0$ but disappears for $L < 1.0$, corresponding to the lower shear layer separation from the leading for $L \geq 1.0$ and from the trailing edge for $L < 1.0$, respectively (Figs. 3 and 4).

4.3 Pressure distribution on the cylinder surface ($\overline{C}_P$)

The time-averaged surface pressure ($\overline{C}_P$) distributions along the cylinder periphery for different P at an intermediate $L = 0.5$ and a large $L = 1.5$ are presented in Figs. 7(a) and 7(b). The $\overline{C}_P$ for $P = 0$ does not change appreciably along the surfaces of the cylinder, very similar to that for a creeping flow. For $P \geq 1$, $\overline{C}_P$ distribution is greatly affected by P; $\overline{C}_P$ is negative for all the surfaces except the front one, which is a general $\overline{C}_P$-distribution characteristics for a square cylinder subjected to a uniform flow (Alam *et al.* 2002). Presently, there is a suction occurring at the lower front-corner of the cylinder. As P is increased, the stagnation point shifts towards the upper front-corner of the cylinder, hence the flow is accelerated for a longer length on the lower-front surface, resulting in the suction pressure. It is more pronounced for larger P. It is noted that the difference in $\overline{C}_P$ between the front and rear surface increases with an increase in P, which leads to a higher drag for a higher P. On the top and bottom surfaces, more negative $\overline{C}_P$ is observed with an increase in P. The difference in $\overline{C}_P$ distribution is associated with the wake vorticity structure. The pressure distribution is affected more on the top surface compared to the bottom surface due to a higher nonlinear flow over the upper surface. At $L = 1.5$, $P = 3$ and 5, the pressure recovery is substantial on the upper side surface (Fig. 7(b)). This is because of the reattachment of the upper shear layer near the trailing edge of the cylinder.
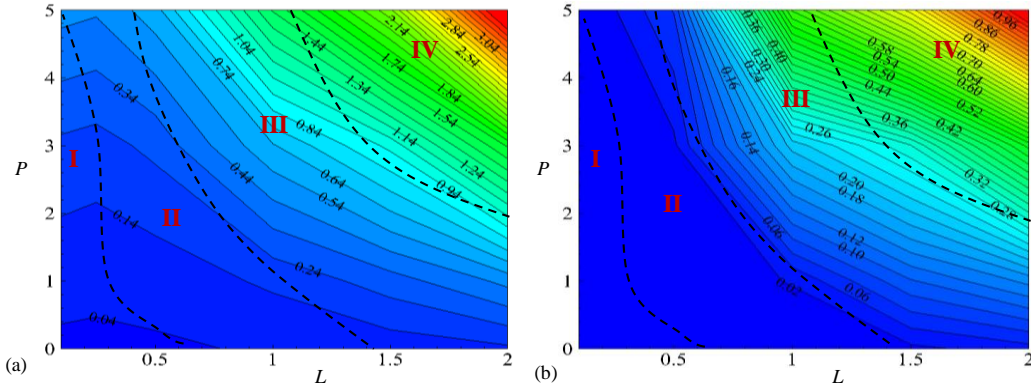
Fig. 8 Contours of (a) time-averaged drag coefficients ($\overline{C}_D$) and (b) rms lift coefficient (C_L'). The dashed lines represent the boundaries between the regimes

Fig. 7(c) shows $\overline{C}_P$ distributions in the gap region of the cylinder, along the lower surface of the cylinder and along the plane wall at different L for a particular $P = 3$. For $L = 0.25$, the difference between $\overline{C}_P$ at the cylinder surface and wall is almost zero. This implies that the gap flow is unidirectional, and the core flow resembles that of a channel flow. As a result, the interaction between the shear layers of the cylinder is lost (Fig. 3). The $\overline{C}_P$ distribution changes with an increase in L for $L \geq 0.5$ where the $\overline{C}_P$ is always higher on the wall than on the bottom surface of the cylinder. This explains why the flow exiting from the gap goes upward, leading to a strong coupling between the upper and lower shear layers of the cylinder (Fig. 4).

4.4 Time-averaged drag coefficient ($\overline{C}_D$) and fluctuating lift coefficient (C_L')

Contours of $\overline{C}_D$ and fluctuating (rms) lift coefficient (C_L') of the cylinder on the L-P plane are shown in Fig. 8. The flow regimes are also marked in the figure. The $\overline{C}_D$ is always positive on the entire L-P plane as expected. The $\overline{C}_D$ boosts when P and/or L is increased, being maximum in regime IV. The boost in $\overline{C}_D$ is substantial in regimes III and IV. The value of $\overline{C}_D$ is very small in regimes I and II as the flow is steady for the former regime and vortices from the lower side rapidly dissipate for the latter regime. As such, at a small L, the pressure difference between the front and rear faces of the cylinder is small (Fig. 7), resulting in the small $\overline{C}_D$. As can be seen from Fig. 7, when P is increased at a particular L, the pressure difference between the front and rear surface enhances which contributes to the increased $\overline{C}_D$.

The variation in C_L' on the L-P plane again distinguishes the flow regimes. The C_L' is zero in regime I because of the steady flow and small in regime II as anticlockwise vortex is absent in the wake. On the other hand, the C_L' in regime III is larger than that in regime II but smaller than that in regime IV. It is consistent with the fact that stretched and regular vortices from the gap appear for regimes III and IV,

respectively. Again, an increased P and/or L corresponds to an increased C_L', the increase is however large in regimes III and IV.

A strong relationship is observed between the flow regimes (presence of vortices) and the values of $\overline{C}_D$ and C_L'. The regimes are classified based on vortices in the wake, i.e., $W_{U,0+L,0}$, $W_{U,R+L,0}$, $W_{U,R+L,S}$ and $W_{U,R+L,R}$; the presence, regularity and size of vortices obviously enhance with the flow regime changing from $W_{U,0+L,0}$ to $W_{U,R+L,R}$. As such, $\overline{C}_D$ and C_L' also grow when the flow regime changes from $W_{U,0+L,0}$ to $W_{U,R+L,R}$.

4.5 Vortex shedding frequency and spectra

Power spectra of lift coefficients of the cylinder as functions of L and P are presented in Fig. 9, where the horizontal axis is normalized based on U and a^*. For the conditions ($L = 0.1$, $P = 0 - 5$; $L = 0.25$; $P = 0 - 3$; and $L = 0.5$, $P = 0$), the flow was steady, and there was no peak in the power spectra. Power spectrum results for these conditions are not presented here. For other values of L and P, at least one definite peak is observed in the spectra. As seen in Fig. 9(a), for $P = 0$, one single predominant peak, marked by St, is identified. The peak heightens with increasing L. There are some ripples around the peak for $W_{U,R+L,S}$ wake but nor for $W_{U,R+L,0}$. The difference might be due to the presence of the stretched vortex for the former. The St for $P = 1$ (Fig. 9(b)) is greater than that for $P = 0$, again the peaks for $W_{U,R+L,S}$ are accompanied by ripples. For higher values of P and L where the wake and wall vortex interaction results in a complicated wake with regular vortices from the upper side and from the gaps (Fig. 4), a peak at $2St$ along with the predominant peak at St characterizes $W_{U,R+L,R}$ wake. Obviously, the different wakes are distinguished by different power spectrum characteristics.

Fig. 10 presents the global view of St variations as a function of P and L. The dominant peak frequency in the power spectra is pondered as the St. The St augments with P for a given L (Fig. 10) corresponding to the shrink in vortex formation length with increasing P (Fig. 4).
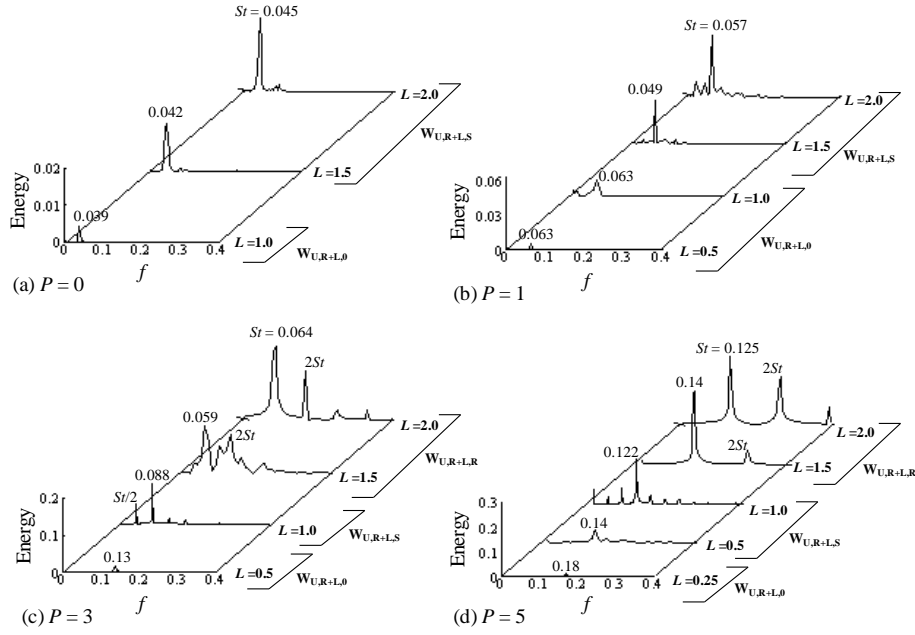
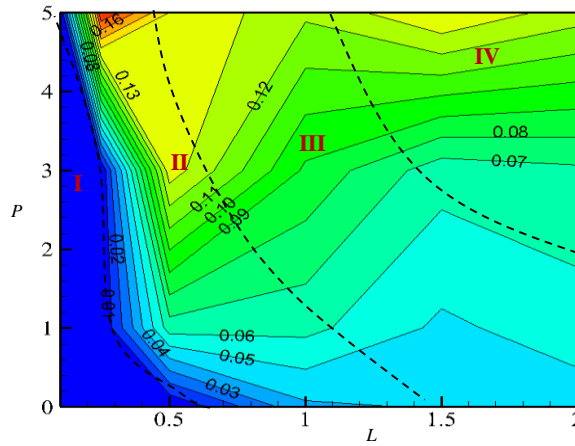Fig. 9 The power spectra of fluctuating lift coefficient at different P and L

Fig. 10 Contours of Strouhal number (St) at different L and P. The dashed lines represent the boundaries between the regimes

The correspondence between formation length and St can be found in Bloor (1964), Alam *et al*. (2011), and Zheng and Alam (2017). The augmentation largely occurs in regime II, the maximum St (= 0.18) occurring $L = 0.25$, $P = 5$, where the wake consists of a single row of regular vortices. While less sensitive to L for a smaller P (< 2), the St is more sensitive to L for a larger P (> 2), though generally declining with L for both small and large P.

5. Conclusions

The effect of gap height (L) and inlet-flow nonlinearity (Couette-Poiseuille pressure gradient P) on the flow structure around a square cylinder is numerically investigated for $L = 0.25 - 2.0$ and $P = 0 - 5$. Results of vorticity, time-mean drag coefficient $\overline{C_D}$, fluctuating (rms) lift coefficient (C_L'), power spectrum of lift, and Strouhal number St are presented. The flow structure is found to be highly sensitive to both P and L. Four distinct flow regimes (I, II, III and IV) are identified based on P and L. Regime I ($W_{U,0+L,0}$) is characterised by a steady flow, appearing at small L, for example at $L \leq 0.5$ for $P = 0$. The critical L value decreases from 0.5 to 0.1 as P increases from 0 to 5. Regime II ($W_{U,R+L,0}$), appearing at a lager L than regime I, features single-row vortex street where vortices from the upper side of the cylinder survive and those from the gap between the cylinder and wall disappear. When P and/or L increases, regime II is followed by Regime III ($W_{U,R+L,S}$) where vortices from the gap are not regular in size but

stretched while those from the upper side is regular. Regime IV (W$_{U,R+L,R}$) prevails at a high P and L, characterized by regular vortices from both upper side and gap.

Following the flow structure dependence on P and L, the aerodynamic parameters $\overline{C}_D$, C_L', and St vary greatly with change in L and/or P. The $\overline{C}_D$ and C_L' both enlarge with increasing P and/or L, being maximum in regime IV and minimum in regime I. The values of $\overline{C}_D$ and C_L' follow the vortex appearance (W$_{U,0+L,0}$, W$_{U,R+L,0}$, W$_{U,R+L,S}$, W$_{U,R+L,R}$) in the wake. As such, a strong relationship is observed between the flow regimes and the values of $\overline{C}_D$ and C_L'. The $\overline{C}_D$ and C_L' also grow with the flow regime changing from W$_{U,0+L,0}$ to W$_{U,R+L,R}$.

Power spectra of lift forces reflect different features at different flow regimes. While no peak appears for regime I, a single peak appears for regime II. For regimes III and IV, the predominant peak is accompanied by some ripples and another peak at superharmonics, respectively. The St grows with P for a given L, the growth largely occurring in regime II. The maximum St is observed as 0.18 at $L = 0.25$, $P = 5$. The St is less sensitive to L for a smaller P (< 2) and more sensitive to L for a larger P (> 2).

For steady flow (regime I), the velocity profile takes a parabolic shape, maximum velocity occurring the near the middle of the gap. For the unsteady flow (regimes II, III and IV), the maximum velocity shifts to the lower surface of the cylinder. When the shear layer is separated from the lower leading edge, there is a region of recirculating flow (negative velocity) near the lower surface of the cylinder. The recirculating flow is absent when the shear layer is attached and separates from the trailing edge.

For a square cylinder in a uniform flow the $\overline{C}_P$ is positive on the front surface and negative on the other three surfaces. For a cylinder in non-uniform flow with a large P where the stagnation point moves sufficiently away from the nominal stagnation point, negative pressure is possible on the lower-front surface of the cylinder because of the flow accelerating for a longer length on the lower-front surface. An increase in P affects the pressure distribution more on the top surface than on bottom surface while an increase in L does the opposite.

Acknowledgments

References

Alam, M.M. and Zhou, Y. (2013), "Intrinsic features of flow around two side-by-side square cylinders", *Phys. Fluids*, **25**, 085106-21.

Alam, M.M., Moriya, M., Takai, K. and Sakamoto, H. (2002), "Suppression of fluid forces acting on two square prisms in tandem arrangement by passive control of flow", *J. Fluid. Struct.*, **16**, 1073-1092.

Alam, M.M., Zhou, Y. and Wang, X.W. (2011), "The wake of two side-by-side square cylinders", *J. Fluid Mech.*, **669**, 432-471.

Bailey, S.C.C., Kopp, G.A. and Martinuzzi, R.J. (2002), "Vortex shedding from a square cylinder near a wall", *J. Turbulence*, **3**, 003.

Bhattacharyya, S. and Maiti, D.K. (2004), "Shear flow past a square cylinder near a wall", *Int. J. Eng. Sci.*, **42**, 2119-2134.

Bhattacharyya, S. and Maiti, D.K. (2005), "Vortex shedding from a square cylinder in presence of a moving wall", *Int. J. Numer. Meth. Fl.*, **48**, 985-1000.

Bhattacharyya, S., Maiti, D.K. and Dhinakaran, S. (2006), "Influence of buoyancy on vortex shedding and heat transfer from a square cylinder in wall proximity", *Numer. Heat Tr, Part A*, **50**(6), 585-606.

Bloor, S.M. (1964), "The transition to turbulence in the wake of a circular cylinder", *J. Fluid Mech.*, **19**, 290-309.

Cao, S., Zhou, Q. and Zhou, Z. (2014), "Velocity shear flow over rectangular cylinders with different side ratios", *Comput. Fluids*, **96**, 35-46.

Cheng, M., Tan, S.H.N. and Hung, K.C. (2005), "Linear shear flow over a square cylinder at low Reynolds number", *Phys. Fluids*, **17**, 078103.

Cheng, M., Whyte, D.S. and Lou, J. (2007), "Numerical simulation of flow around a square cylinder in uniform shear flow", *J. Fluid. Struct.*, **23**, 207-226.

Davis, R.W. and Moore, E.F. (1982), "A numerical study of vortex shedding from rectangles", *J. Fluid Mech.*, **116**, 475-506.

Davis, R.W., Moore, E.F. and Purtell, L.P. (1984), "A numerical-experimental study of confined flow around rectangular cylinders", *Phys. Fluids,* **27**, 46-59.

Dhinakaran, S. (2011), "Heat transport from a bluff body near a moving wall at Re=100", *Int. J. Heat Mass Trans.*, **54**, 5444-5458.

Franke, R., Rodi, W. and Schonung, B. (1990), "Numerical calculation of laminar vortex shedding flow past cylinders", *J. Wind Eng. Aerod.*, **35**(1-3), 237-257.

Hwang, R.R. and Sue, Y.C. (1997), "Numerical simulation of shear effect on vortex shedding behind a square cylinder", *Int. J. Numer. Meth. Fl.*, **25**, 1409-1420.

Islam, S.U., Zhou, C.Y., Shah, A. and Xie, P. (2012), "Numerical simulation of flow past rectangular cylinders with different aspect ratios using the incompressible lattice Boltzmann method", *J. Mech. Sci. Tech.*, **26**, 1027-1041.

Kumaran, M. and Vengadesan, S. (2007), "Flow characteristics behind rectangular cylinder placed near a wall", *Numer. Heat Tr.-A*, **52**, 643-660.

Lankadasu, A. and Vengadesan, S. (2008), "Onset of vortex shedding in planar shear flow past a square cylinder", *Int. J. Heat Fluid Fl.*, **29**, 1054-1059.

Lee, B.S., Kim, T.Y. and Lee, D.H. (2005), "Control of vortex shedding behind a rectangular cylinder near the ground", *Numer. Heat Tr.-A*, **47**, 787-804.

Leonard, B.P. (1995), "Order of accuracy of QUICK and related convection–diffusion Schemes", *Appl. Math. Model.*, **19,** 640-653.

Li, Z., Lan, C., Jia, L. and Ma, Y. (2017), "Ground effects on separated laminar flows past an inclined flat plate", *Theor. Comp. Fluid Dyn.*, **31**, 127-136.

Maiti, D.K. (2011), "Dependence of flow characteristics of rectangular cylinders near a wall on the incident velocity", *Acta Mech*, **222**, 273-286.

Maiti, D.K. (2012), "Numerical study on aerodynamic characteristics of rectangular cylinders near a wall", *Ocean Eng.*, **54**, 251-260.

Maiti, D.K. and Bhatt, R. (2015), "Interactions of vortices of a square cylinder and a rectangular vortex generator under Couette Poiseuille flow", *J. Fluids Eng. – ASME*, **137**, 051203-1.

Martinuzzi, R.J., Bailey, S.C.C.R. and Kopp, G.A. (2003), "Influence of wall proximity on vortex shedding from a square cylinder", *Exp. Fluids,* **34**, 585-596.

Patankar, S.V. (1980), "*Numerical Heat Transfer and Fluid Flow*". Hemisphere Publishing Corporation, Taylor and Francis Group, New York.

Rastan, M.R., Sohankar, A. and Alam, M.M. (2017), "Low-Reynolds-number flow around a wall-mounted square cylinder: flow structures and onset of vortex shedding", *Phys. Fluids*, **29**, 103601-19.

Samani, M. and Bergstrom, D.J. (2015), "Effect of a wall on the wake dynamics of an infinite square cylinder", *Int. J. Heat Fluid Fl.*, **55**, 158-166.

Schlichting, H. and Gersten, K. (2000), "Boundary-Layer Theory", Springer, New York.

Sohankar, A. (2008), "Large eddy simulation of flow past rectangular-section cylinders: side ratio effects", *J. Wind Eng. Aerod.*, **96**, 640-655.

Sohankar, A., Norberg, C. and Davidson, L. (1997), "Numerical simulation of unsteady low-Reynolds number flow around rectangular cylinders at incidence", *J. Wind Eng. Aerod.*, **69**, 189-201.

Wang, X.K. and Tan, S.K. (2008), "Comparison of flow patterns in the near wake of a circular cylinder and a square cylinder placed near a plane wall", *Ocean Eng*., **35**, 458-472.

Yu, D., Butler, K., Kareem, A., Glimm, J. and Sun, J. (2013), "Simulation of the Influence of aspect ratio on the aerodynamics of rectangular prisms", *J. Eng. Mech. - ASCE*, **139**, 0733-9399.

Zheng, Q. and Alam, M.M. (2017), "Intrinsic features of flow past three square prisms in side-by-side arrangement", *J. Fluid Mech*., **826**, 996-1033.

Zovatto, L. and Pedrizzetti, G. (2001), "Flow about a circular cylinder between parallel walls", *J. Fluid Mech*., **440**, 1-25.